Magnetocaloric effect in magnetothermally-responsive nanocarriers for hyperthermia-triggered drug release

2012 Nanotechnology 23 505706

(http://iopscience.iop.org/0957-4484/23/50/505706)

Nanotechnology **23** (2012) 505706 (10pp) doi:10.1088/0957-4484/23/50/505706

Magnetocaloric effect in magnetothermally-responsive nanocarriers for hyperthermia-triggered drug release

Jianbo Li[1], Yang Qu[1], Jie Ren[1], Weizhong Yuan[1] and Donglu Shi[2,3]

[1] Institute of Nano- and Bio-polymeric Materials, School of Material Science and Engineering, Tongji University, 4800 Caoan Road, Shanghai 201804, People's Republic of China
[2] School of Electronic and Computing Systems, University of Cincinnati, Cincinnati, OH, 10 45221, USA
[3] The Institute for Biomedical Engineering and Nano Science, School of Medicine, Tongji University, 1239 Siping Road, Shanghai 200092, People's Republic of China

E-mail: quyang-tongji@163.com and renjie6598@163.com

Received 1 September 2012, in final form 22 October 2012
Published 26 November 2012
Online at stacks.iop.org/Nano/23/505706

Abstract
The magnetocaloric effects and lower critical solution temperature (LCST) were investigated in a magnetothermally-responsive nanocarrier for magnetothermal drug release under alternating magnetic field (AMF). The $Mn_{0.2}Zn_{0.8}Fe_2O_4$ nanoparticles with low T_c were dispersed in a polymeric matrix consisting of *N*-Isopropyl acrylamide (NIPAAm) and *N*-hydroxymethyl acrylamide (HMAAm). The magnetocaloric effects and LCST of the nanocarriers were characterized by using high-resolution electron transmission microscopy, thermogravimetric analyses, and vibrating sample magnetometer. The maximum self-heating temperature of 42.9 °C was achieved by optimizing the $Mn_{0.2}Zn_{0.8}Fe_2O_4$ concentration in the polymer matrix. By adjusting the NIPAAm to HMAAm ratio, the LCST was controlled at an ideal level of 40.1 °C for efficient thermosensitive drug delivery. Magnetothermally responsive drug release of Doxorubicin, an anticancer drug, was significantly enhanced by application of an external AMF on the nanocarriers. The cytotoxicity experimental results *in vitro* show good biocompatibility and efficient therapeutic effects in cancer treatment.

(Some figures may appear in colour only in the online journal)

1. Introduction

In tumor therapy, several stimuli-responsive nanocarriers have been developed with various triggering strategies based on environmental changes, such as enzymes, pH, light, and temperature [1–4]. Among all stimuli-responsive drug deliveries, the thermosensitive nanocarrier has been known for its combined advantage of hyperthermia [5]. Hyperthermia was reported to enhance permeability of tumor vasculature, leading to high uptake of the nanocarriers in lesions [6]. Furthermore, it can also enhance chemotherapy by increased drug cytotoxicity [7–9]. However, the great challenge has been on the design of a unique nanostructure capable of both efficient hyperthermia treatment of tumors and targeted thermochemotherapy. The delivery nanosystem also needs to be biocompatible and clinically viable.

As a typical inverse thermosensitive polymer, poly (*N*-isopropylacrylamide) (PNIPAAm) has been utilized as a drug-loaded carrier. PNIPAAm exhibits a lower critical solution temperature (LCST) around 32 °C, which is close to body temperature [10]. For desirable thermosensitive drug delivery at the physiological temperature (37 °C), LCST

should be slightly above it (∼40 °C). Therefore, a critical step in the nanocarrier design is to have the LCST of the system controlled in the range of 40 °C–45 °C. It has been found that the LCST of thermosensitive polymer can be varied by addition of appropriate hydrophilic monomers, such as N, N'-dimethylacrylamide (DMAAm) or N-hydroxymethylacrylamide (HMAAm) [11, 12]. By adjusting the ratio of NIPAAm to hydrophilic monomers, the LCST of random copolymer can readily change from 40 °C to 45 °C.

In targeted drug release, both spatial–temporal targeting and temperature control have been great challenges. In traditional approaches, heating may be divided into bodily and regional heating in clinics [13]. The former can be achieved mainly by hot water baths or perfusion with heated blood, which lacks selectivity [13]. Ultrasound, near-infrared (NIR), and electromagnetism have been used for more energy-focused treatments [14–17]. Among them, nanoparticle-mediated NIR and electromagnetic hyperthermia have been studied extensively for the advantages of simultaneous imaging and hyperthermia [18, 19]. In phototherapy, the treatment is often disadvantaged by limitation of light penetration.

The magnetic nanoparticle (MNP) mediated hyperthermia has been demonstrated to exhibit clinical effectiveness and spatial–temporal accuracy under an alternating magnetic field (AMF) due to hysteresis loss and/or Néel relaxation [20, 21]. For magnetic hyperthermia treatment, the field can easily penetrate the human tissues without adverse effects. The uptake of the MNPs in lesions can be achieved by a strong permanent gradient magnetic field, known as magnetic drug targeting (MDT) [22, 23]. MNPs have also been widely employed as contrast agents for magnetic resonance imaging (MRI) [24]. Thus, MNPs can serve as ideal candidates for drug delivery, targeting, imaging, and hyperthermia therapy simultaneously.

The temperature control in AMF is critical in drug release by nanocarriers. In general, hyperthermia raises the tissue temperature between 40.0 °C and 44.0 °C in order to kill cancerous cells while preserving the normal cells [25, 26]. Recent *in vivo* studies have demonstrated that the thermal enhancement of cytotoxicity is maximized at temperatures between 40.5 °C and 43 °C for several chemotherapeutic agents [27]. Therefore, it is necessary to control the maximum self-heating temperature around 43 °C for the magnetothermally-responsive drug delivery system. As an intrinsic property of the magnetic materials, the Curie temperature (Curie point, T_c) can be utilized to regulate the magnetocaloric effect of the nanoparticles [28, 29]. However, the T_c of most commercially available MNPs, such as Fe_3O_4 with T_c of 860 K, is much higher than the body temperature [30]. For a system to work in a clinically viable temperature range, magnetic materials with low T_c values are preferred. Mn–Zn ferrite ($Mn_{1-x}Zn_xFe_2O_4$) is one of the MNPs with high magnetic permeability and low core losses. It is also well known that the properties of these ferrite materials are strongly influenced by their compositions and microstructures. By substitution of nonmagnetic Zn^{2+} ions instead of the magnetic Mn^{2+} ions, the corresponding T_c can be lowered from 463 K ($Mn_{0.9}Zn_{0.1}Fe_2O_4$) to 361 K ($Mn_{0.5}Zn_{0.5}Fe_2O_4$) under AMF [31]. It was found in our previous study that, with Mn to Zn ratios of 8:2, 6:4, 4:6, and 2:8, the corresponding T_c values of $Mn_{1-x}Zn_xFe_2O_4$ were 235, 171, 112, and 89 °C respectively [32].

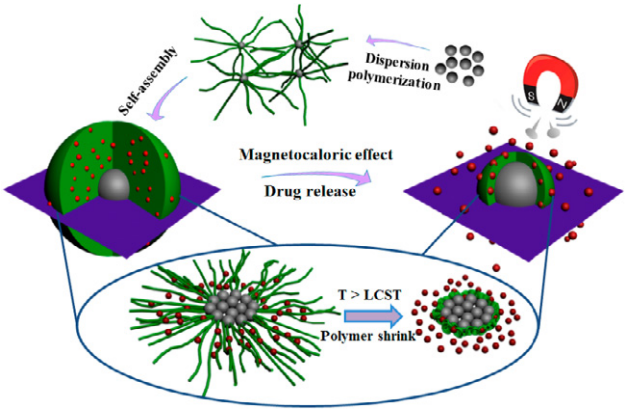

Figure 1. Schematic illustration showing the preparation process of the nanocarriers and mechanism of magnetothermal drug release.

In this study, a magnetothermally-responsive nanocarrier is designed and developed as shown in figure 1. In this figure, the thermosensitive copolymers are composed of NIPAAm and HMAAm. The Mn–Zn ferrite nanoparticles are embedded in the polymeric matrix. For clinical viability and safety, the $Mn_{0.2}Zn_{0.8}Fe_2O_4$ nanoparticle is employed as its low T_c is close to body temperature. The thermosensitive copolymers, with LCST around 40 °C, are prepared by adjusting the NIPAAm to HMAAm ratio. The mass fraction of Mn–Zn ferrite nanoparticle is varied to control the maximum temperature for drug delivery under AMF. The maximum self-heating temperature and the LCST of the nanocarrier are controlled in an appropriate temperature range (40–44 °C). It is noted that the maximum self-heating temperature should be slightly higher than LCST in order to trigger thermosensitive drug release completely under AMF (see figure 1). Furthermore, water-soluble anticancer drug doxorubicin (Dox) is loaded in the nanocarrier for investigation of the magnetothermally-responsive drug release mechanism. Cytotoxicity is also investigated for both magnetothermally-responsive nanocarriers and Dox-nanocarriers.

2. Experimental details

2.1. Materials

Manganese chloride ($MnCl_2 \cdot 4H_2O$), zinc chloride ($ZnCl_2$ anhydrous), ferric chloride ($FeCl_3$ anhydrous), dimethyl sulfoxide (DMSO), Poly (N-vinylpyrrolidone) (PVP; weight-average molecular weight 24,000), N, N'-methylene-bisacrylamide (MBAAm), N-hydroxymethylacrylamide-(HMAAm) and ammonium persulfate (APS) were purchased from Shanghai Chemical Reagent Co., LTD. N, N'-isopropylacrylamide (NIPAAm) was purchased from TCI.

Doxorubicin hydrochloride (Dox · HCl) was provided by XinHua Hospital (Shanghai, China). Dulbecco minimum essential medium (DMEM), fetal bovine serum (FBS), and 3-(4, 5-Dimethylthiazol-2-yl)-2, 5-diphenyltetrazolium bromide (MTT) were purchased from Invitrogen corporation (USA). HMAAm was further purified by recrystallization from chloroform twice before use. NIPAAm was purified by recrystallization from hexane and toluene. DMSO were dried over CaH_2 and distilled before use. Other reagents were commercially available and were used as received.

2.2. Preparation of $Mn_{0.2}Zn_{0.8}Fe_2O_4$ nanoparticles

$Mn_{0.2}Zn_{0.8}Fe_2O_4$ nanoparticles were selected for their suitable magnetocaloric effect, and prepared by wet chemical co-precipitation method as a magnetic precursor [32, 33]. In detail, aqueous solutions of 0.2 M manganese chloride ($MnCl_2 \cdot 4H_2O$), 0.8 M zinc chloride ($ZnCl_2$ anhydrous), and 2 M solution of ferric chloride ($FeCl_3$ anhydrous) were mixed to form a solution. This mixed solution was diluted with 800 ml of deionized water under vigorous stirring. Then 5 M NaOH in the boiling state was added into the solution quickly in order to set the pH at 11.5–12. The solution was kept at ∼100 °C for 60 min under vigorous stirring. The precipitate was washed several times with distilled water until neutrality, then collected by an external magnetic field and dried in a vacuum oven at room temperature.

2.3. Preparation of P(NIPAAm-co-HMAAm)-$Mn_{0.2}Zn_{0.8}Fe_2O_4$ nanocarriers

The dispersion polymerization method was used to prepare the magnetothermally-responsive nanocarriers. The nanocarriers were synthesized with the $Mn_{0.2}Zn_{0.8}Fe_2O_4$ nanoparticles. They were added in the monomer mixtures prior to polymerization. MBAAm was used as a crosslinking agent to prevent the dissolution of P(NIPAAm-*co*-HMAAm) in water.

In order to adjust the thermosensitive property of the nanocarriers, the ratios of NIPAAm to HMAAm were set to be 5:1 (435 mg, 3.85 mmol/78 mg, 0.77 mmol), 7:1 (452 mg, 3.99 mmol/58 mg, 0.57 mmol), and 9:1 (469 mg, 4.14 mmol/47 mg, 0.46 mmol) with $Mn_{0.2}Zn_{0.8}Fe_2O_4$ loading of 8% (50 mg). Typically, in a 100-ml one-neck round-bottom flask equipped with a magnetic stirring bar, MBAAm (60 mg, 0.4 mmol), 0.2 g PVP, 20 mg APS, and certain amount of NIPAAm/HMAAm with the ratios mentioned above were dissolved in 50 ml of distilled water. Five milliliters of $Mn_{0.2}Zn_{0.8}Fe_2O_4$ ferrofluid (10 mg ml^{-1}) were added. The mixture was then degassed by three freeze–thaw–pump cycles in a nitrogen atmosphere, and heated to 70 °C to start the polymerization. The reaction proceeded under stirring (400 rpm) for 8 h at 70 °C. After completion of polymerization, the carrier was separated magnetically and thoroughly washed with distilled water several times to remove unreacted monomer, nonmagnetic particles, and other impurities.

In order to adjust the magnetothermal property of the nanocarriers, nanoparticle loadings of 6% (37.5 mg), 8% (50 mg), and 10% (62.5 mg) of the gross weight of the monomer and cross-linker were selected with a NIPAAm to HMAAm ratio of 7:1. Similar nanocarriers with different $Mn_{0.2}Zn_{0.8}Fe_2O_4$ loadings were prepared by the same process described above. Finally, these products were freeze-dried and stored under vacuum at 18 °C.

2.4. Characterization of $Mn_{0.2}Zn_{0.8}Fe_2O_4$ nanoparticles and nanocarriers

2.4.1. X-ray diffraction (XRD). The structural formation of $Mn_{0.2}Zn_{0.8}Fe_2O_4$ was characterized by XRD with a Rigaku D/Max-2550VB3+ (Japan, Cu Kα radiation, 40 kV, 100 mA).

2.4.2. The high-resolution transmission electron microscopy (HRTEM). HRTEM was conducted by JEOL JEM-2010F (Japan, 200 KV) to observe the morphology of the $Mn_{0.2}Zn_{0.8}Fe_2O_4$ nanoparticles and nanocarriers. The $Mn_{0.2}Zn_{0.8}Fe_2O_4$ nanoparticles were dispersed into deionized water by ultrasonic sound. A drop of the solution was placed on a copper grid and left to dry before transferring into the TEM sample chamber. In order to observe the polymer in the nanocarriers, the specimen was prepared by drying a drop of nanocarrier solution on a copper grid coated with amorphous carbon. A small drop of phosphotungstic acid (PTA) solution (2 wt% in deionized water) was deposited onto the copper grid. After drying, the morphology of the nanocarriers was observed by TEM.

2.4.3. Fourier transform infrared (FT-IR) spectrometry. Fourier transform infrared (FT-IR) spectrometry (Bruker Equinox55 FT-IR spectrometer, Germany) was employed to study the formation of the nanocarriers. The specimens were pressed into potassium bromide pellets.

2.4.4. Dynamic laser scattering (DLS). The thermosensitive properties of the nanocarriers with different NIPAAm to HMAAm ratios were characterized by dynamic laser scattering (DLS). DLS measurements were made using a Malvern Autosizer 4700 (UK). The dried specimen was dispersed in deionized water (0.2 mg ml^{-1}), sonicated and analyzed for the size distribution. The thermosensitive properties of the nanocarriers with different NIPAAm to HMAAm ratios were determined by measuring the nanoparticle sizes at different temperatures. The specimens were allowed to equilibrate for 1 min at set temperatures before measurement.

2.4.5. Thermogravimetric analyses (TGA). The contents of $Mn_{0.2}Zn_{0.8}Fe_2O_4$ nanoparticles in the carriers with different MNP loadings were determined by thermogravimetric analyses (TGA). TGA tests of the specimens with different MNP loadings were conducted using a NETZSCH STA 449C (Germany) with the temperature range from 25 °C to 600 °C and a heating rate of 10 °C min^{-1}. The TGA specimens were prepared by drying under vacuum oven for solvent removal.

2.4.6. Vibrating sample magnetometer (VSM). The magnetic hysteresis curves of $Mn_{0.2}Zn_{0.8}Fe_2O_4$ nanoparticles and nanocarriers with different MNP loadings were obtained at room temperature by using a vibrating sample magnetometer (VSM) (LakeShore 7404 vibrating sample magnetometer, USA). The applied magnetic field was in the range 0–2 T.

2.4.7. Magnetothermal property. The heat generation of $Mn_{0.2}Zn_{0.8}Fe_2O_4$ nanoparticles and the nanocarriers was achieved by using an AC magnetic field generator (Nanjing University Instrument Plant WG). The concentration of the suspensions in deionized water was adjusted to 5 mg ml^{-1} and the volume of each specimen was 5 ml. The conditions of the alternating magnetic field irradiation were fixed at 360 kHz and 6.5 kA m^{-1}.

2.5. Preparation and in vitro cytotoxicity of Dox-nanocarriers

The Dox-nanocarriers was prepared following a previously published protocol [34]. Typically, 5 mg Dox-HCl and 45 mg of nanocarriers with $Mn_{0.2}Zn_{0.8}Fe_2O_4$ nanoparticle loadings of 8% and NIPAAm/HMAAm ratios of 7/1, were completely dissolved in 20 ml deionized water by ultrasonication for 10 min. The brown glass vial was sealed and shaken overnight at 25 °C to facilitate Dox uptake in the swelling shell of the nanocarrier. After loading, the Dox-nanocarrier was magnetically separated and freeze-dried. The whole procedure was performed in the dark.

The Drug loading content (DLC) was calculated according to the following formula [35]:

$$\text{DLC(wt\%)} = [\text{weight of Dox/weight of Dox-nanocarrier}] \times 100\%.$$

2.6. Characterization of Dox-nanocarriers

2.6.1. Investigation of Drug loading content (DLC). To investigate the DLC of the drug-loaded carriers, Dox content in the supernatant and freeze-dried Dox-nanocarrier was determined by a UV/Vis spectrophotometer (Hitachi U-3310, Japan) and compared with the standard absorption curve of Dox in deionized water at 480 nm.

2.6.2. Drug release behavior of the Dox-nanocarriers in an external AMF. The effect of AMF on drug release of the Dox-nanocarrier was investigated. The thermosensitive-related drug release behaviors were studied at different temperatures (43 °C and 37 °C) as control.

Briefly, dried Dox-nanocarriers were dispersed ultrasonically in PBS (pH = 7.4) at a concentration of 5 mg ml^{-1}. Without AMF, 2 ml Dox-nanocarrier solution was dialyzed against 40 ml PBS at different temperatures (43 °C and 37 °C) for 24 h (MWCO: 3500, Shanghai Chemical Reagent Co., China). At predetermined time intervals, 4 ml media was extracted from a dialysis bag outside and replaced with fresh PBS. Dox content in the extracted solution was measured by UV/Vis spectrophotometry and the cumulative Dox release was calculated.

The magnetothermal drug release was performed with a similar procedure as for thermosensitive-related drug release behaviors described above with an external AMF. Briefly, 20 ml Dox-nanocarrier solution (5 mg ml^{-1}) was placed in a double wall vacuum bottle, which was irradiated by an intermediate frequency alternating magnetic field generator at 360 kHz and 6.5 kA m^{-1}. At predetermined time intervals, as described above on thermosensitive-related drug release at a fixed temperature, 0.5 ml Dox-nanocarrier solution was extracted and dialyzed against 10 ml PBS for 30 min at 20 °C. The Dox content of the extracted solution was measured by UV/Vis spectrophotometry.

2.6.3. Cytotoxicity of nanocarriers and anti-tumor activity of Dox-nanocarriers in vitro. *In vitro* cytotoxicity was evaluated by MTT assay. QBC cells (a human cholangiocarcinoma cell) were placed onto 96-well plates at 2.0×10^3 cell density and incubated with DMEM (containing 10% FBS) for 24 h. The cells were then exposed to DMEM with serial concentrations of the Dox-nanocarrier and pure nanocarrier. At the same time, the cells were subjected to DMEM with free Dox (5 μg ml^{-1}) and without being selected as positive and negative control. After 48 h, the cells were washed with PBS and incubated with DMEM again for another 6 h. Then, the cell mediums were replaced with DMEM containing MTT (5 mg ml^{-1}) for another 4 h and replaced again with DMSO. The optical densities (OD) were read at 490 nm using microtiter plate reader (BIO-RAD, USA).

The cell viability was calculated by the following equation:

$$\text{Cell viability} = (\text{OD value of a specimen/OD value of the negative control}) \times 100\%.$$

The average IC_{50} (50% cell viability concentration) of the Dox-nanocarrier was estimated based on the MTT results. The MTT test was carried out in three replicates and each time five wells of cells were used for each specimen.

The influence of the Dox-nanocarrier and plain nanocarrier on apoptotic was reflected directly by Hoechst 33 258 staining assay. Briefly, after incubating with the Dox-nanocarriers (100 μg ml^{-1}) and pure nanocarriers (400 μg ml^{-1}) for 48 h, the cells were washed with PBS twice, then incubated with Hoechst 33 258 (5 μg ml^{-1}) at room temperature for 5 min. At the end of incubation, cells were rinsed three times with PBS. Finally, the treated cells were observed using a fluorescence microscope (Olympus IX 71, Japan).

3. Results and discussion

3.1. The formation and physiochemical characterization of the $Mn_{0.2}Zn_{0.8}Fe_2O_4$ nanoparticle

The results of XRD, as shown in figure 2, indicate the single-phase spinel structure, matching well with JCPDS card

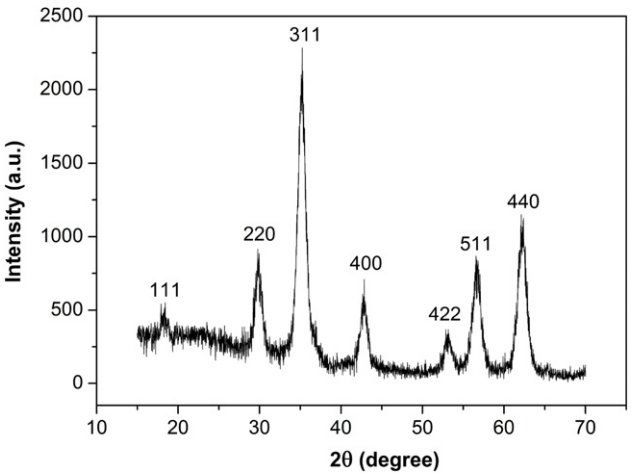

Figure 2. The XRD spectrum of $Mn_{0.2}Zn_{0.8}Fe_2O_4$.

74-2399 for $Mn_{0.2}Zn_{0.8}Fe_2O_4$. The peaks at 18.5, 30.2, 35.6, 43.0, 53.4, 57.1 and 62.5° are well indexed to the crystal plane of spinel ferrite (111), (220), (311), (400), (422), (511), and (440), respectively. Figure 3(a) is the HRTEM (high-resolution transmission electron microscopy) image, showing the spherical morphology of a $Mn_{0.2}Zn_{0.8}Fe_2O_4$ nanoparticle with diameter around 7 nm. The $Mn_{0.2}Zn_{0.8}Fe_2O_4$ nanoparticles are superparamagnetic at room temperature, with a saturation magnetization of 32.4 emu g^{-1}, as shown in figure 4(a). The apparatus used for *in vitro* heat generation is schematically depicted in figure 5(a), which supplies AMF of 80 kHz and 6.5 kA m^{-1}. The self-heating curve under AC indicated that the self-heating temperature of $Mn_{0.2}Zn_{0.8}Fe_2O_4$ nanoparticles could increase up to around 56 °C and reached a plateau after about 6 min, as shown in figure 5(b).

3.2. Formation and physiochemical characterization of $Mn_{0.2}Zn_{0.8}Fe_2O_4$ nanocarriers

3.2.1. HRTEM result of nanocarriers. Figures 3(b) and (c) are TEM images of the nanocarriers with 8% $Mn_{0.2}Zn_{0.8}Fe_2O_4$. As can be seen in this figure, the nanocarriers exhibit spherical morphology with the $Mn_{0.2}Zn_{0.8}Fe_2O_4$ nanoparticles embedded in the polymer matrix. Furthermore, EDAX (energy dispersive analysis of x-rays) data shown in figure 3(d) are consistent with the presence of Fe, Mn, and Zn in the polymer matrix.

3.2.2. FT-IR result of nanocarriers. Figure 6 shows the FT-IR spectrum of the MNP and nanocarriers. The two other peaks observed at 462 and 580 cm^{-1} in figures 6(a) and (b) are assigned to the M–O bond ($M = Mn^{2+}$, Zn^{2+} and Fe^{3+}), which proved the existence of Mn–Zn ferrite. However, comparing with the spectrum of Mn–Zn ferrite, two new peaks

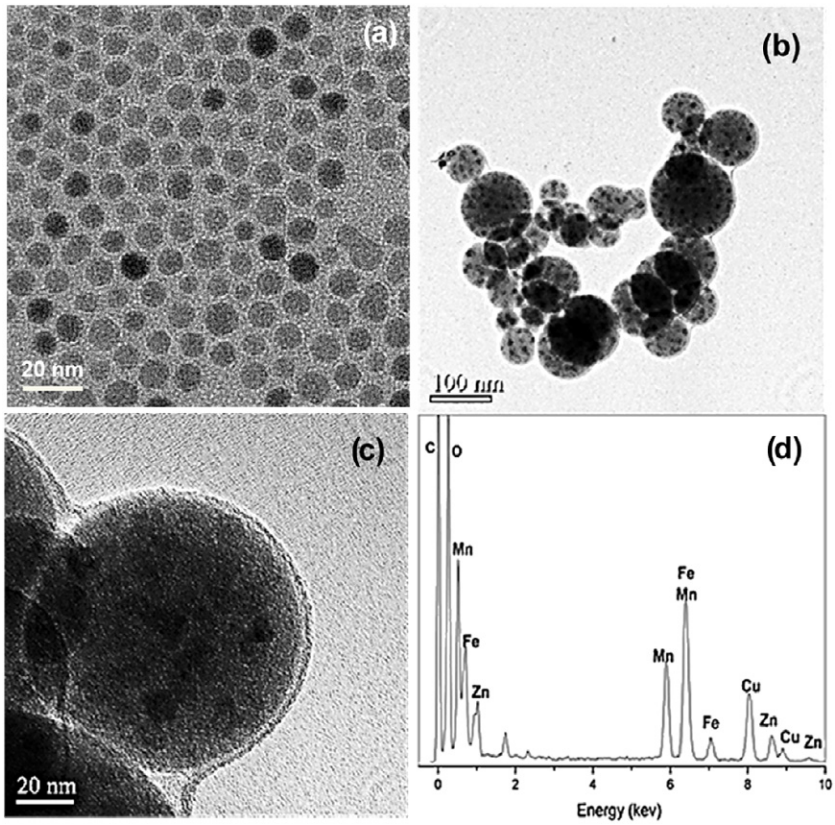

Figure 3. The morphologies and elemental compositions of $Mn_{0.2}Zn_{0.8}Fe_2O_4$ and nanocarriers with 8% $Mn_{0.2}Zn_{0.8}Fe_2O_4$ loading: (a) the HRTEM of $Mn_{0.2}Zn_{0.8}Fe_2O_4$ nanoparticles; (b) and (c) the HRTEM of nanocarriers; (d) the EDAX result of nanocarriers.

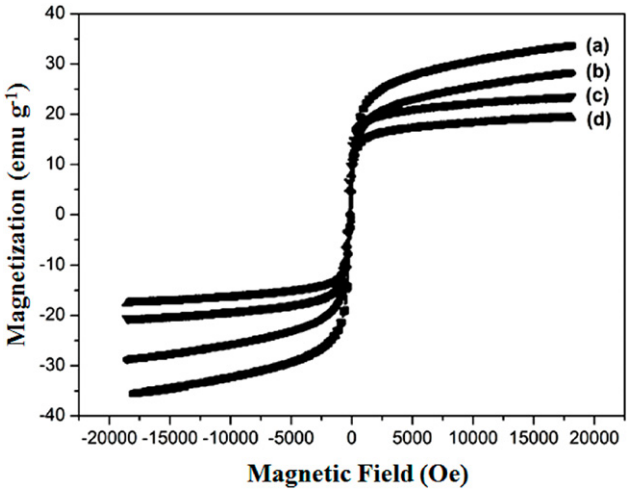

Figure 4. The magnetization curves of $Mn_{0.2}Zn_{0.8}Fe_2O_4$ nanoparticles and nanocarriers with different MNP loadings at room temperature for field strengths up to 20 kOe: (a) $Mn_{0.2}Zn_{0.8}Fe_2O_4$; (b) nanocarriers with 10% $Mn_{0.2}Zn_{0.8}Fe_2O_4$ loading; (c) nanocarriers with 8% $Mn_{0.2}Zn_{0.8}Fe_2O_4$ loading; (d) nanocarriers with 6% $Mn_{0.2}Zn_{0.8}Fe_2O_4$ loading.

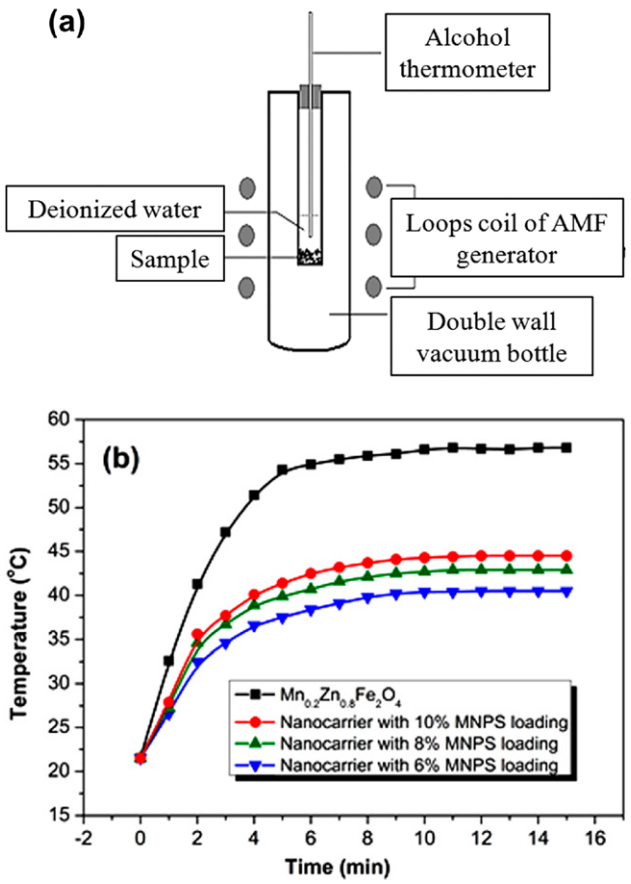

Figure 5. (a) Schematic illustration of magnetically induced self-heating system. (b) Self-heating characteristics of $Mn_{0.2}Zn_{0.8}Fe_2O_4$ nanoparticles and nanocarriers with different $Mn_{0.2}Zn_{0.8}Fe_2O_4$ loading dispersed in water and subjected to a 80 kHz and 6.5 kA m^{-1} alternating magnetic field. Ambient temperature = 22 °C. Ferrofluid concentration = 5 mg ml^{-1}, volume = 5 ml.

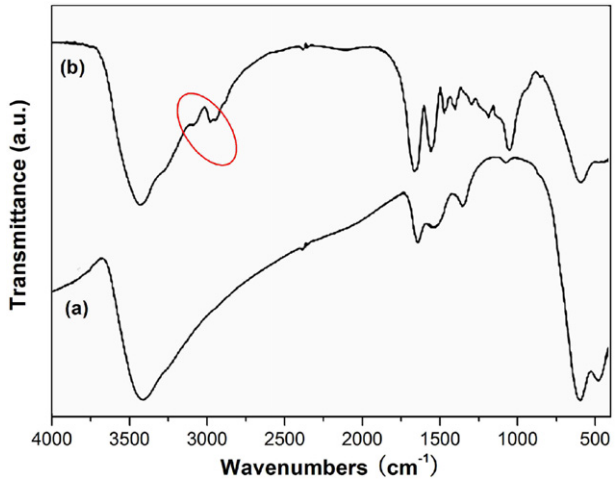

Figure 6. FT-IR spectrum of $Mn_{0.2}Zn_{0.8}Fe_2O_4$ and nanocarriers: (a) $Mn_{0.2}Zn_{0.8}Fe_2O_4$; (b) nanocarriers.

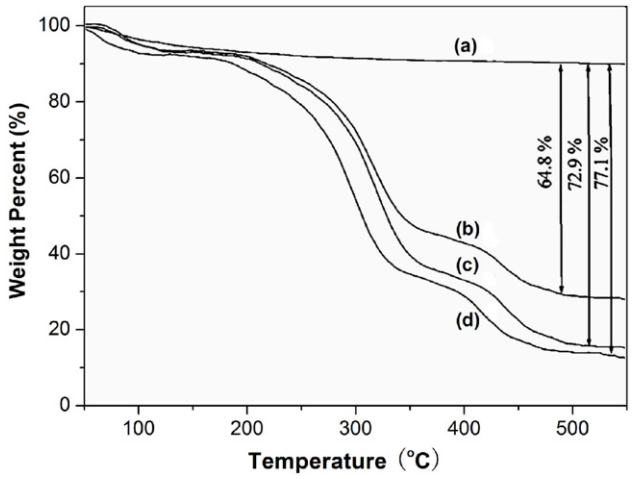

Figure 7. TGA curves of $Mn_{0.2}Zn_{0.8}Fe_2O_4$ nanoparticles and nanocarriers with different MNP loadings: (a) $Mn_{0.2}Zn_{0.8}Fe_2O_4$; (b) nanocarriers with 10% $Mn_{0.2}Zn_{0.8}Fe_2O_4$ loading; (c) nanocarriers with 8% $Mn_{0.2}Zn_{0.8}Fe_2O_4$ loading; (d) nanocarriers with 6% $Mn_{0.2}Zn_{0.8}Fe_2O_4$ loading.

appear between 3000 and 2800 cm^{-1} in figure 6(b), which respectively represent asymmetric and symmetric vibration modes of CH_2 and CH_3. It is well known that CH_2 and CH_3 are the main compositions of the polymer, which did not exist in Mn–Zn ferrite nanoparticles. Also nonmagnetic pure polymer was completely removed by repeated magnetic separation. Therefore, the two peaks appearing between 3000 and 2800 cm^{-1}, highlighted by the red circle in figure 6(b), imply the polymer had been grafted on the surface of the magnetic nanoparticles.

3.2.3. TGA result of nanocarriers. Figure 7 shows the thermogravimetric analysis (TGA) data of the weight losses between 200 °C and 550 °C, which correlate to the polymer mass fractions in the nanocarriers. These losses: 77.1%, 72.9%, and 64.8%, as shown in figure 7, are corresponding to the different $Mn_{0.2}Zn_{0.8}Fe_2O_4$ loadings of 6%, 8% and

10%, respectively. A similar trend in MNP content variation was reported by Purushotham *et al* [36]. However, the $Mn_{0.2}Zn_{0.8}Fe_2O_4$ nanoparticle ratios in the carrier were higher than those feed ratios. This is attributable to nucleation of nonmagnetic polymers taking place separately from the MNPs and removed during magnetic separation.

3.3. Appropriate magnetic, thermosensitive and magnetothermal properties of nanocarriers by adjusting component ratio

3.3.1. Magnetic properties of nanocarriers. The strong effects of $Mn_{0.2}Zn_{0.8}Fe_2O_4$ loading on the nanocarriers can be seen in figure 4. The magnetization curves (figures 4(b)–(d)) show the saturation magnetizations of the nanocarriers to be 26.7, 22.1, and 17.9 emu g^{-1}, which correspond to mass fractions of the $Mn_{0.2}Zn_{0.8}Fe_2O_4$ of 10%, 8% and 6% in the nanocarriers. Consistently, these values are lower that of the pure $Mn_{0.2}Zn_{0.8}Fe_2O_4$ nanoparticles (32.4 emu g^{-1} as shown in figure 4(a)).

3.3.2. Thermosensitivity of nanocarriers. The thermosensitivity of the nanocarriers was investigated by DLS analyses, as shown in figure 8. As a result of a phase transition in PNIPAAm, the thermosensitive nanocarrier experiences a sharp coil–globule phase transition in water, transforming from an expanded hydrophilic structure below LCST to a compact hydrophobic structure above it. Therefore, the shell of the nanocarrier is in a shrinkage state, leading to the reduction of the nanocarriers' hydrodynamic diameter in water at temperatures above LCST (see schematic illustration in figure 1) [37]. The behavior has been observed by DLS, reflecting the size change of the nanoparticles in deionized water. The LCST values of nanocarriers with HMAAm molar ratios of 9:1, 7:1, and 5:1 are estimated to be 36.7 °C, 40.1 °C, and 41.2 °C respectively.

3.3.3. Magnetothermal properties of nanocarriers. One of the key features of the nanocarriers is the control of drug release, tuned by the self-heating temperature. Figure 5(b) shows the self-heating curves of the $Mn_{0.2}Zn_{0.8}Fe_2O_4$ nanoparticles and their nanocarrier counterparts with varied mass fractions of $Mn_{0.2}Zn_{0.8}Fe_2O_4$ under an AC field. These curves indicate those nanocarriers with various mass fractions of MNP exhibit similar behaviors as for $Mn_{0.2}Zn_{0.8}Fe_2O_4$ nanoparticles, however, at much lower increasing rates and temperature ranges. For the nanocarriers with MNP loadings of 10%, 8%, 6% in deionized water, the corresponding temperatures have increased up to 44.5 °C, 42.9 °C, 40.5 °C and reached steady state within 6–10 min. The result indicated the excellent magnetocaloric properties of the nanocarriers, including rapid calefactive velocity and maintenance of the temperature.

Based on the above results, the magnetothermally-responsive nanocarriers can be optimized with a PNIPAAm to HMAAm ratio of 7:1 and a $Mn_{0.2}Zn_{0.8}Fe_2O_4$ nanoparticles loading of 8%, for the most efficient magnetothermal drug release. These are advantages ideally suited for clinical applications, particularly in terms of biological safety and physiological tolerance without using a temperature probe and controller [38].

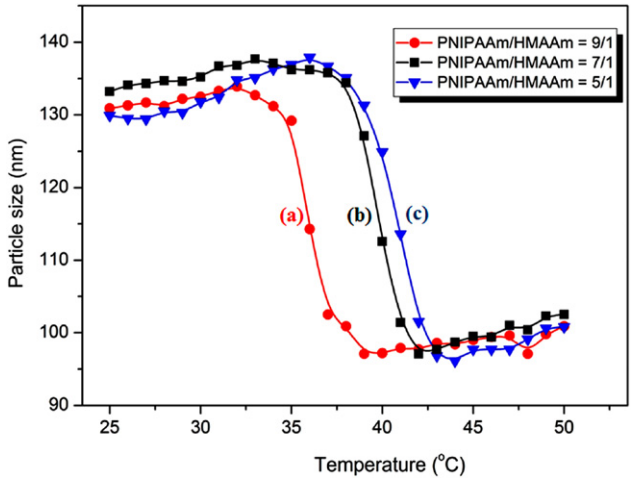

Figure 8. DLS results for nanocarriers with different ratios of PNIPAAm/HMAAm: (a) nanocarriers with ratio of PNIPAAm/HMAAm as 9/1; (b) nanocarriers with ratio of PNIPAAm/HMAAm as 7/1; (c) nanocarriers with ratio of PNIPAAm/HMAAm as 5/1.

3.4. In vitro magnetothermal drug release, stability and cytotoxicity of the nanocarriers

3.4.1. DLC and in vitro magnetothermal drug release of nanocarriers. Nanocarriers with optimum LCST (40.1 °C) and pronounced magnetocaloric effect (42.9 °C) were selected for *in vitro* tests. The UV–visible spectrophotometry results show a 4.26 wt% drug loading in the Dox-nanocarrier.

The controlled drug release of Dox-nanocarrier was studied in PBS (pH = 7.4) under different conditions. The magnetothermal drug release was examined in an external AMF with the fixed parameters. As control, different temperatures (37 °C and 43 °C) were used to simulate the drug release of thermosensitive nanocarriers in physiological conditions and hyperthermia, respectively.

The accumulative doxorubicin release (%) from the drug carrier under these conditions is presented in figure 9. At 37 °C, the cumulative release of Dox in PBS reaches approximately 35% within 8 h without any further release until 24 h. At 43 °C, the cumulative release of Dox in PBS is approximately 86% within 4 h, and up to 97% at 12 h. When the Dox-nanocarrier is exposed to an external AMF, the cumulative release of Dox is similar to those at 43 °C, approximately 84.9% within 4 h and 95% at 12 h.

Comparing these three curves in figure 9, it can be seen that the drug accumulative release and initial release rates are much higher for the AFM-enhanced case and that at 43 °C. Since LCST (40.1 °C) of the thermosensitive nanocarriers is higher than 37 °C, the Dox release is mainly dependent on diffusion into the release media (PBS) at physiological temperature. However, in an external AMF, the magnetocaloric effect of the Mn–Zn ferrite core can

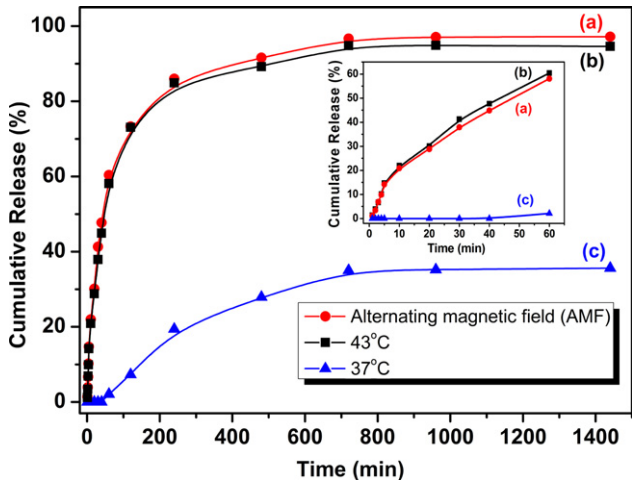

Figure 9. The drug release profiles of Dox-nanocarriers in PBS (pH = 7.4) at different condition: (a) an alternating magnetic field with fixed 80 kHz and 6.5 kA m^{-1}; (b) 43 °C ($T >$ LCST); (c) 37° ($T <$ LCST).

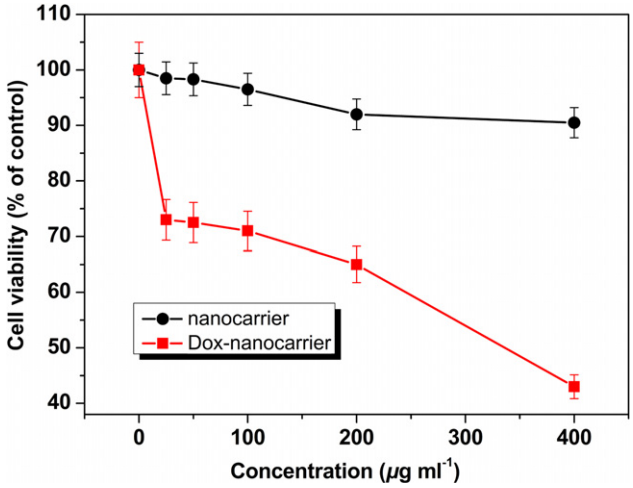

Figure 10. The cytotoxicity study of Dox-nanocarriers and nanocarriers with 8% MNPs loadings and PNIPAAm/HMAAm ratio of 7/1.

induce heat generation, transferred through the polymer shell, causing a local temperature rise above its LCST. Consequently, the shell of nanocarrier collapses, resulting in rapid drug release. Similar results from controlling temperature have been reported in the literature [39–41]. However, thermosensitive drug release by the magnetocaloric effect is a unique approach and a more practical strategy compared to a simple water bath [42–44]. Moreover, the magnetocaloric effect can be controlled by selection of a Mn–Zn ferrite with proper T_c and mass fraction of the $Mn_{0.2}Zn_{0.8}Fe_2O_4$ nanoparticles. The effective control of drug release can also be achieved by an external AMF.

3.4.2. Stability of nanocarriers under different condition. At the same time, the stabilities of the nanocarriers under different conditions were reflected in the drug release experiment. After the Dox-nanocarriers had been dispersed in PBS at 37 °C for 24 h, the solution was transparent without any precipitation. Meanwhile, when the Dox-nanocarriers had been dissolved in PBS at 43 °C after 24 h, the solution became a suspension without obvious precipitation. However, a distinct phenomenon has been observed that nanocarriers had become precipitations completely and arranged along with induction coils under AMF after 1 h. These phenomena showed the nanocarriers had good stability under physiological conditions and excellent magnetic targeting under AMF, which would benefit nanocarriers' application in clinics.

3.4.3. Biological properties of nanocarriers. Cytotoxicities of nanocarriers and Dox-nanocarriers were assessed with free Dox (5 μg ml^{-1}) as positive control and DMEM (containing 10% FBS) as negative control. The QBC cell viability after 48 h incubation with nanocarriers and Dox-nanocarriers at different concentrations, ranging from 0 to 400 μg ml^{-1}, were examined by the MTT method. As shown in figure 10, the nanocarriers exhibit good biocompatibility with a cell viability more than 90% at the highest concentration of 400 μg ml^{-1}. In contrast, the Dox-nanocarriers show strong concentration-dependent cytotoxicity. As the Dox-nanocarrier concentration increases, the cell viability decreases significantly. At a Dox-nanocarrier concentration of 400 μg ml^{-1}, the corresponding cell viability is about 42.8%, which is similar to the result of free Dox (5 μg ml^{-1}, 43.9%, not shown). Although the cytotoxicity of Dox-nanocarriers is much lower than that of the free Dox, the actual content of Dox in nanocarriers (400 μg ml^{-1}) is about 17 μg ml^{-1}. Dox-nanocarriers at a concentration of 400 μg ml^{-1} have been found to release free Dox of 5.9 μg ml^{-1} under the usual cell culture conditions at 37 °C.

The effects of Dox-nanocarriers with different concentrations on QBC cell proliferation were also investigated by fluorescent imaging. Hoechst 33 258 was combined with the cell nuclei as molecular probes for its rapid uptake by living cells. Living cells incorporated with the Hoechst 33 258 dye exhibit blue fluorescence, whereas apoptotic cells and dead cells appear dark, as they are not stained (figure 11). After 24 h incubation with the Dox-nanocarriers (100 and 400 μg ml^{-1}), cell proliferation is inhibited markedly and cell number decreases with the increase of Dox-nanocarrier concentration. Corresponding to the MTT result, cell proliferation is not affected by nanocarriers at a concentration of 400 μg ml^{-1}. As shown in figure 11, the living cell number is close to that in the negative control. These results clearly indicate good biocompatibility and effective drug release of the nanocarriers.

4. Conclusions

Versatile nanocarriers for controlled drug release have been developed based on the magnetothermally triggered mechanism. The nanocarriers are designed to be capable of multifunctionalities in diagnosis and treatment, including cell targeting, imaging, magnetothermal drug release, and thermochemotherapy. A $Mn_{0.2}Zn_{0.8}Fe_2O_4$ nanoparticle, with

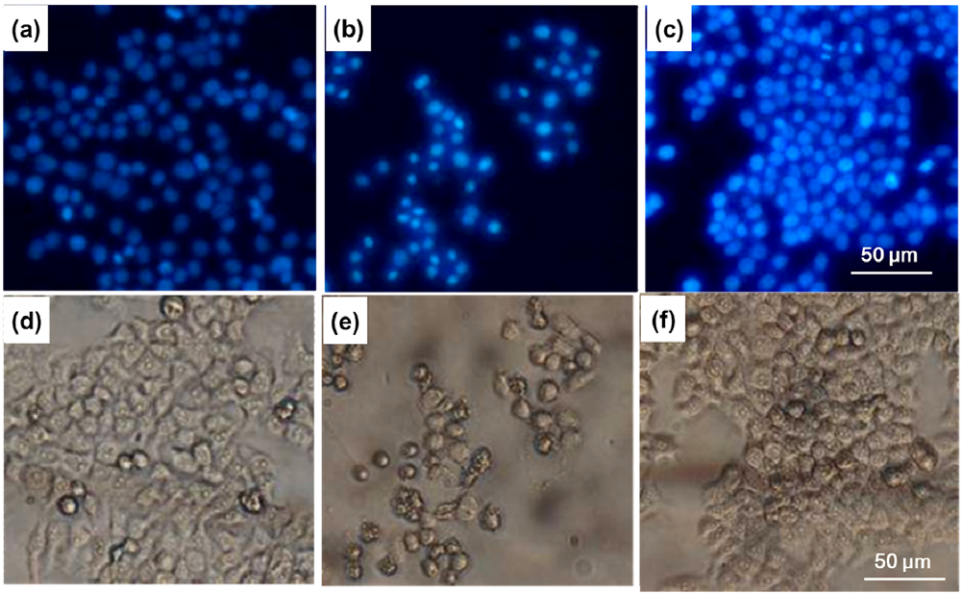

Figure 11. Apoptotic morphological study of QBC cells treated with nanocarriers ((a) and (d), 400 μg ml^{-1}), Dox-nanocarriers ((b) and (e), 100 μg ml^{-1}) and negative control ((c) and (f), DMEM containing 10% FBS): (a)–(c) fluorescence images; (d)–(f) bright-field micrographs.

a low T_c, is identified as the magnetic core. It is well dispersed and embedded in the matrix of the nanocarriers. The concentration of $Mn_{0.2}Zn_{0.8}Fe_2O_4$ nanoparticles in the nanocarriers is optimized to provide a pronounced magnetocaloric effect. A thermosensitive polymer, with optimized LCST, has also been prepared by adjusting the PNIPAAm to HMAAm ratio. A maximum self-heating temperature of 42.9 °C and LCST of 40.1 °C are obtained for an 8% $Mn_{0.2}Zn_{0.8}Fe_2O_4$ nanoparticle loading and a 7:1 PNIPAAm to HMAAm ratio. Under AMF, the temperature of the nanocarriers can be raised to 42.9 °C for triggering thermosensitive 'on–off' switch (LCST at 40.1 °C). This is a critical step for controlled drug release and maintaining a temperature at 42.9 °C for biological safety. The *in vitro* magnetothermal drug release test has shown effective magnetothermal responses of the nanocarrier. An *in vitro* cytotoxicity study of the nanocarrier indicates its good biocompatibility. The magnetothermally responsive nanocarriers present high possibilities in clinical systemic therapeutics with multifunctionalities.

Acknowledgments

We gratefully acknowledge the financial support from the Science and Technology Commission of Shanghai Municipality (No. 11nm0505100), the China Postdoctoral Science Foundation (No. 2012M510116) and the Fundamental Research Funds for the Central Universities (Nos 0500219142, 0500219160).

References

[1] Chandrawati R, Odermatt P D, Chong S F, Price A D, Stadler B and Caruso F 2011 *Nano Lett.* **11** 4958
[2] Kim D, Zhong G G, Lee E S and You H B 2009 *Mol. Pharmacol.* **6** 1353
[3] You J, Shao R, Wei X, Gupta S and Li C 2010 *Small* **6** 1022
[4] Kono K, Ozawa T, Yoshida T, Ozaki F, Ishizaka Y, Maruyama K, Kojima C, Harada A and Aoshima S 2010 *Biomaterials* **31** 7096
[5] Li Y P, Pan S R, Zhang W and Du Z 2009 *Nanotechnology* **20** 065104
[6] Koning G A, Eggermont A M M, Lindner L H and ten Hagen T L M 2010 *Pharm. Res.* **27** 1750
[7] Issels R D 2008 *Eur. J. Cancer* **44** 2546
[8] Issels R D 1999 *Onkologie* **22** 374
[9] Hildebrandt B, Wust P, Ahlers O, Dieing A, Sreenivasa G, Kerner T, Felix R and Riess H 2002 *Crit. Rev. Oncol. Hematol.* **43** 33
[10] Schild H G 1992 *Prog. Polym. Sci.* **17** 163
[11] Nakayama M, Okano T, Miyazaki T, Kohori F, Sakai K and Yokoyama M 2006 *J. Control. Release* **115** 46
[12] Cheng C, Wei H, Shi B X, Cheng H, Li C, Gu Z W, Cheng S X, Zhang X Z and Zhuo R X 2008 *Biomaterials* **29** 497
[13] Wust P, Hildebrandt B, Sreenivasa G, Rau B, Gellermann J, Riess H, Felix R and Schlag P M 2002 *Lancet Oncol.* **3** 487
[14] Dromi S, Frenkel V, Luk A, Traughber B, Angstadt M, Bur M, Poff J, Xie J, Libutti S K, Li K C P and Wood B J 2007 *Clin. Cancer Res.* **13** 2722
[15] Park J, Maltzahn G, Ong L L, Centrone A, Hatton T A, Ruoslahti E, Bhatia S N and Sailor M J 2010 *Adv. Mater.* **22** 880
[16] Silva A C *et al* 2011 *Int. J. Nanomed.* **6** 591
[17] Kita E, Hashimoto S, Kayano T, Minagawa M, Yanagihara H, Kishimoto M, Yamada K, Oda T, Ohkohchi N and Takagi T 2010 *J. Appl. Phys.* **107** 09B321
[18] Chen C L, Kuo L R, Chang C L, Hwua Y K, Huang C K, Lee S Y, Chen K, Lin S J, Huang J D and Chen Y Y 2010 *Biomaterials* **31** 4104
[19] Sharma R and Chen C 2009 *J. Nanopart. Res.* **11** 671
[20] Hergt R, Dutz S, Muller R and Zeisberger M 2006 *J. Phys.: Condens. Matter* **18** 2919
[21] Morozy P, Jones S K and Gray B N 2002 *Int. J. Hyperth.* **18** 267
[22] Hua M Y *et al* 2011 *Biomaterials* **32** 8999
[23] Gitter K and Odenbach S 2011 *J. Magn. Magn. Mater.* **323** 3038

[24] Ponce A M, Viglianti B L, Yu D, Yarmolenko P S, Michelich C R, Woo J, Bally M B and Dewhirst M W 2007 *J. Natl Cancer Inst.* **99** 53
[25] Schildkopf P, Ott O J, Frey B, Wadepohl M, Sauer R, Fietkau R and Gaip U S 2010 *Curr. Med. Chem.* **17** 3045
[26] Roti Roti J L 2008 *Int. J. Hyperth.* **24** 3
[27] Sugarbaker P H 2007 *Int. J. Hyperth.* **23** 431
[28] Matsuki H, Satoh T, Murakami K, Hoshino T, Yanada T and Kikuchi S 1999 *IEEE Trans. Magn.* **26** 1551
[29] Settecase F, Sussman M S and Roberts T 2007 *Contrast Media Mol. Imaging* **2** 50
[30] Ortiz E C, Perez O P, Voyles P, Gutierrez G and Tomar M S 2009 *Microelectron. J.* **40** 677
[31] Nica V, Sauer H M, Embs J and Hempelmann R 2008 *J. Phys.: Condens. Matter* **20** 204115
[32] Cao Y, Ren J, Li J B and Liu Y 2011 *J. Biomater. Sci.* **22** 1473
[33] Cao Y, Ren J, Li J B and Liu Y 2010 *Mater. Lett.* **64** 1570
[34] Purushotham S and Ramanujan R V 2010 *Acta Biomater.* **6** 502
[35] Sun Y, Yan X, Yuan T, Liang J, Fan Y, Gu Z and Zhang X 2010 *Biomaterials* **31** 7124
[36] Purushotham S, Chang P E, Rumpel H, Kee I, Ng R, Chow P, Tan C and Ramanujan R V 2009 *Nanotechnology* **20** 305101
[37] Zhang J and Misra R D K 2007 *Acta Biomater.* **3** 838
[38] Todaka T, Kishino T and Enokizono M 2010 *J. Magn. Magn. Mater.* **320** E702
[39] Zhao A, Zhou S, Zhou Q and Chen T 2010 *Pharm. Res.* **27** 1627
[40] Li L, Hagen T L M, Schipper D, Wijnberg T M, Rhoon G C, Eggermont A M, Lindner L H and Koning G A 2010 *J. Control. Release* **143** 274
[41] Li W, Li J, Gao J, Li B, Xia Y, Meng Y, Yu Y, Chen H, Dai J and Wang H 2011 *Biomaterials* **32** 3832
[42] Pradhan P, Giri J, Rieken F, Koch C, Mykhaylyk O, Döblinger M, Banerjee R, Bahadur D and Plank C 2010 *J. Control. Release* **142** 108
[43] Katagiri K, Imai Y, Koumoto K, Kaiden T, Kono K and Aoshima S 2011 *Small* **7** 1683
[44] Brazel C S 2009 *Pharm. Res.* **26** 644